THE ASTRONOMICAL JOURNAL, 121:517–524, January 2001

POTENTIAL OF ASTROGRAPHIC PLATES FOR STELLAR FLARE DETECTION

A. FRESNEAU
Observatoire astronomique, UMR 7550, 11 rue de l'Université, F-67000 Strasbourg, France
R. W. ARGYLE
Institute of Astronomy, University of Cambridge, Madingley Road, Cambridge, CB3 0HA, England, UK
AND
G. MARINO AND S. MESSINA
Osservatorio Astrofisico di Catania, Università di Catania, via S. Sofia 78, I-95125 Catania, Italy
Received 2000 June 28; accepted 2000 September 28

ABSTRACT

A set of four test regions covering a total celestial area of 520 deg^2 at low galactic latitude is investigated on a set of 130 century-old astrographic plates. About 8% of the 2×10^5 stars with apparent B magnitude 10–14 and with total proper-motion component larger than $0''.02$ yr^{-1} show a significant flickering greater than 0.4 mag in B over a timescale shorter than 20 minutes. About 25% of these stellar flare candidates concern stars with $B-V \sim 0.2$ (spectral type A7). A procedure to select pre–main-sequence stellar candidates from the distance-limited sample of 16×10^3 disk dwarfs with detected flickering in B magnitude ≥ 0.4 is presented in view of a mass loss of $10^{-8}\ M_\odot$ yr^{-1}, derived from the analysis of the angular momentum distribution of stellar orbits. Follow-up UBV photoelectric photometry at the present epoch of 200 nearby stellar flares along the Vulpecula Rift shows an effect of reddening in $B-V$ and of blueing in $U-B$ for about 10% of the targets. The detection of optically thin or thick disks around the selected targets is suggested.

The success rate in detecting optical flares in nearby stars of $\sim 1.5\ M_\odot$ with as much as $5 \times 10^{-6}\ M_\odot$ dumped onto the central star during the past 100 years, from deep astrographic plates coupled with 1 m–class telescope is estimated to 10% with a kinematical bias that can be dealt with.

Key words: stars: flare — surveys

1. ASTROGRAPHIC OBSERVATIONS

Flare stars were discovered accidentally in 1949 when photographic plates with multiple exposures were used on a routine basis for variable star detection (Luyten 1949). Since the 10,000 deep astrographic plates of the Astrographic Program were exposed through a similar technique of multiple exposures at the beginning of the 20th century, the purpose of the present paper is to check the potential of this century-old all-sky survey whose main goal was restricted to provide charts down to a photographic magnitude of 14.5 (Mouchez 1887, 755). From the historical perspective of this all-sky survey, we want to point out that the technique for printing maps at the end of the 19th century was to engrave a copper plate from the photographic plate enlarged 2 times and then produce paper charts directly from the etched copper plate. A triple exposure on the photographic plate was meant to provide an asterism that discriminates real stellar images from possible plate defects in processing long ($\sim$90 minutes) exposures. While not all the paper charts were produced, the original photographic plates are still accessible from 15 plate vaults worldwide. The paper charts proved to be even more accurate than the transit instrument observations made at that time (Turner 1900).

Thanks to modern digitized sky surveys going much deeper than the 14.5 mag limit set by the goals of the Astrographic Program, it is possible to convert the magnitude-limited sample of the deep astrographic plates into a volume-limited sample when using the total proper motion as an indication for distance (Fresneau 1990). The availability of fast measuring machines devoted to Schmidt telescope plate scanning proves that 1 μm and 0.1 mag accuracies in the geometric and radiometric calibrations of photographic plates is achievable. The present study benefits from the experiences of the large bulk of Schmidt plates already scanned with these fast machines.

The test regions that we are using are selected in Delphinus (Table 1) and in Gemini (Table 2), where we do not observe large regions of interstellar material and regions along the Vulpecula Rift (Fresneau & Monier 1999), and in Cygnus (Table 3), where we observe large regions of dust and gas along the Great Dark Rift. All these regions are at low galactic latitude, where proper-motion components in galactic latitude are sensitive to the deflection of the velocity perpendicular to the galactic disk. The proper-motion components in galactic longitude in regions with galactic longitudes $l = 180°$ (in Gemini) and $l \leq 60°$ (in Delphinus) are sensitive to the differential galactic rotation. We cannot detect any expansion effect in the galactic disk due to a lack of radial velocities for the stellar sample under study, but we can investigate the angular momentum distribution around the z-axis perpendicular to the galactic disk once we know the distance from the Sun, and we assume $R_\odot = 8.5$ kpc and $V_\odot = 225$ km s^{-1} for the rotation of the Galaxy at the Sun's location.

The epoch of the earliest astrographic plates in the present study is 1898, while the latest is 1933. The time for each exposure was set up to reach a magnitude limit of 14.5 and was fixed at 20 or 30 minutes (30 minutes for the Paris astrographic instrument, 20 minutes for the Bordeaux and Brussels astrographic instruments). The time for each of the three exposures was set identical to 20 or 30 minutes but we noticed in our study the well-known effects of the photographic emulsion nonlinear sensitivity, which tends to over-

TABLE 1

LIST OF ASTROGRAPHIC PLATES IN DELPHINUS

α	12°	14°	16°	18°	20°	22°	24°
20 08.....	1911 Aug 18	1929 Aug 18	1901 Apr 08	1909 Aug 23	1907 Aug 27	1902 Sep 08	1899 Sep 09
20 16.....	1921 Aug 30	1907 Sep 06	1904 Sep 08	1911 Jul 26	1919 Aug 30	1907 Jul 30	1898 Sep 06
20 24.....	1923 Jul 19	1909 Jul 21	1904 Sep 05	1920 Sep 19	1907 Aug 12	1907 Aug 01	1899 Sep 05
20 32.....	1920 Sep 10	1909 Oct 10	1922 Sep 22	1910 Aug 10	1919 Jul 30	1933 Jul 26	1898 Sep 13
20 40.....	1912 Oct 12	1922 Sep 22	1909 Jul 24	1909 Aug 11	1907 Aug 10	1904 Aug 03	1899 Sep 04
20 48.....	1923 Jul 19	1912 Oct 14	1904 Sep 04	1909 Aug 23	1920 Oct 09	1906 Jul 27	1898 Sep 09

NOTES.—Units of right ascension are hours and minutes. Astrographic plates obtained with the Paris Observatory astrographic instrument ($\delta = 18°, 20°, 22°, 24°$; three 30 minute exposures) and the Bordeaux astrographic instrument ($\delta = 12°, 14°, 16°$; three 20 minute exposures), scanned with the MAMA (Paris plates) and the APM (Bordeaux plates).

expose the images close to bright targets or those taken first in the series of three exposures.

2. STELLAR FLARE CANDIDATES CATALOG

We used three different machines—the Automatic Plate Measuring Facility (APM) in Cambridge[1] (England), the Automated Plate Scanner (APS) in Minneapolis,[2] and the Machine A Mesurer pour l'Astronomie (MAMA)[3] in Paris—in exactly the same way they are routinely used on Schmidt plates, and we were pleased to find the same kind of 1 μm repeatability on century-old plates. We wish to

[1] See http://www.ast.cam.ac.uk~mike/casu/apm/apm.html.

[2] See http://aps.umn.edu/.

[3] See http://dsmama.obspm.fr/.

TABLE 2

LIST OF ASTROGRAPHIC PLATES IN GEMINI

α	14°	16°	18°	20°	22°
05 36.....	1914 Jan 22	1908 Jan 23	...	...	...
05 44.....	1913 Feb 26	1911 Jan 26	...	...	...
05 52.....	1913 Feb 10	1910 Dec 28	1921 Mar 10	1920 Nov 21	1907 Jan 04
06 00.....	1911 Mar 01	1910 Jan 31	1920 Jan 23	1921 Mar 08	1903 Jan 05
06 08.....	1911 Feb 21	1910 Jan 02	1921 Mar 09	1911 Jan 31	1908 Jan 23
06 16.....	1914 Jan 30	1911 Feb 02	...	...	...
06 24.....	1921 Dec 29	1910 Feb 09	...	...	...

NOTE.—Selected astrographic plates obtained with the Paris Observatory astrographic instrument ($\delta = 18°, 20°, 22°$; three 30 minute exposures) and the Bordeaux astrographic instrument ($\delta = 14°, 16°$; three 30 minute exposures) in the galactic anticenter region, scanned with the MAMA (Bordeaux plates) and the APS (Paris plates).

TABLE 3

LIST OF ASTROGRAPHIC PLATES IN CYGNUS

α	33°	35°	37°	39°
19 55.....	...	...	1923 Aug 08	1925 Aug 17
20 01.....	1911 Aug 18	1929 Aug 18	...	...
20 05.....	...	...	1925 Sep 15	...
20 10.....	1927 Sep 24	1912 Jul 17	...	...
20 15.....	...	...	1925 Sep 13	1929 Aug 30
20 19.....	1925 Oct 10	1911 Aug 23	...	...
20 25.....	...	...	1921 Oct 05	1923 Aug 09
20 28.....	1910 Aug 10	1911 Aug 29	...	...
20 35.....	...	...	1922 Oct 16	1921 Sep 29
20 37.....	1925 Sep 14	...	...	...
20 45.....	...	...	...	1923 Sep 03
20 46.....	...	1921 Sep 07	...	...
20 55.....	1924 Oct 18	1913 Aug 01	...	...
20 55.....	...	...	1925 Sep 21	...
21 04.....	1908 Aug 19	...	...	...
21 05	...	...	1921 Sep 05	1920 Oct 30

NOTE.—Usable astrographic plates around the northern coalsack in Cygnus were obtained with the Brussels Royal Observatory astrographic instrument (three 20 minute exposures) and scanned with the APM.

emphasize that these machines are fast (about 1/2 hr per astrographic plate, less than the observing time that went into the plate almost a century ago), and they provide an automated detection of images [with the (x, y) plate coordinates of the images, the ellipticity, and an integrated density over the plate area for each image], according to well-known tested procedures of a local peak finder in the pixels, such as SExtractor (Bertin & Arenou 1996). The usable size of the astrographic plates is 12 by 12 cm, and the scale is $1'$ mm^{-1}, close to the $67'$ mm^{-1} plate scale of the Schmidt telescopes used in all-sky photographic surveys as early as 1949.

In Figure 1, we show a small, 20 by 20 mm area (plate scale $1'$ mm^{-1}) around NGC 6871 in Cygnus as a plot of the outputs from the APM of the region appearing on one deep plate from Brussels Observatory. The triangles are plotted from an automated procedure written to handle the asterism geometry of triple images (Ortiz-Gil, Hiesgen, & Brosche 1998) and to discriminate stellar images from plate defects. Stellar coordinates and magnitude are computed as the mean values of the triple exposures.

Typical values for the mean square errors are about 2 μm and 0.2 mag for the geometric and radiometric calibrations, respectively, as we concluded from the analysis of the offsets between the three exposures. These results suggest that improvements in analyzing the stellar images over the entire plate area could possibly be made to take full advantage of the potential of the fast measuring machines at the 1 μm level (Abad & Vicente 1999). We did not investigate in the present study, for instance, the asterism stability over the entire 12 $\times$ 12 cm plate, even if the geometric variation between the triple images over the field of view of $2^\circ \times 2^\circ$ can define the optical distortion of the astrographic instrument. Such an analysis should be made once the entire set of about 500 astrographic plates per astrographic instrument is scanned, to derive mean instrumental properties, like the ones established from the short-exposure plates of the Astrographic Catalogue (Urban et al. 1998).

At this point of the analysis, we have for each astrographic plate with a $2^\circ \times 2^\circ$ field of view a catalog of about 4000 stars with positions and magnitudes computed as the mean value of the three images with the mean square errors (on the order of 2 μm and 0.2 mag). We did not investigate the stars that were visible in only two exposures, and we considered stars with a mean square error in magnitude larger than 0.4 as stellar flare candidates.

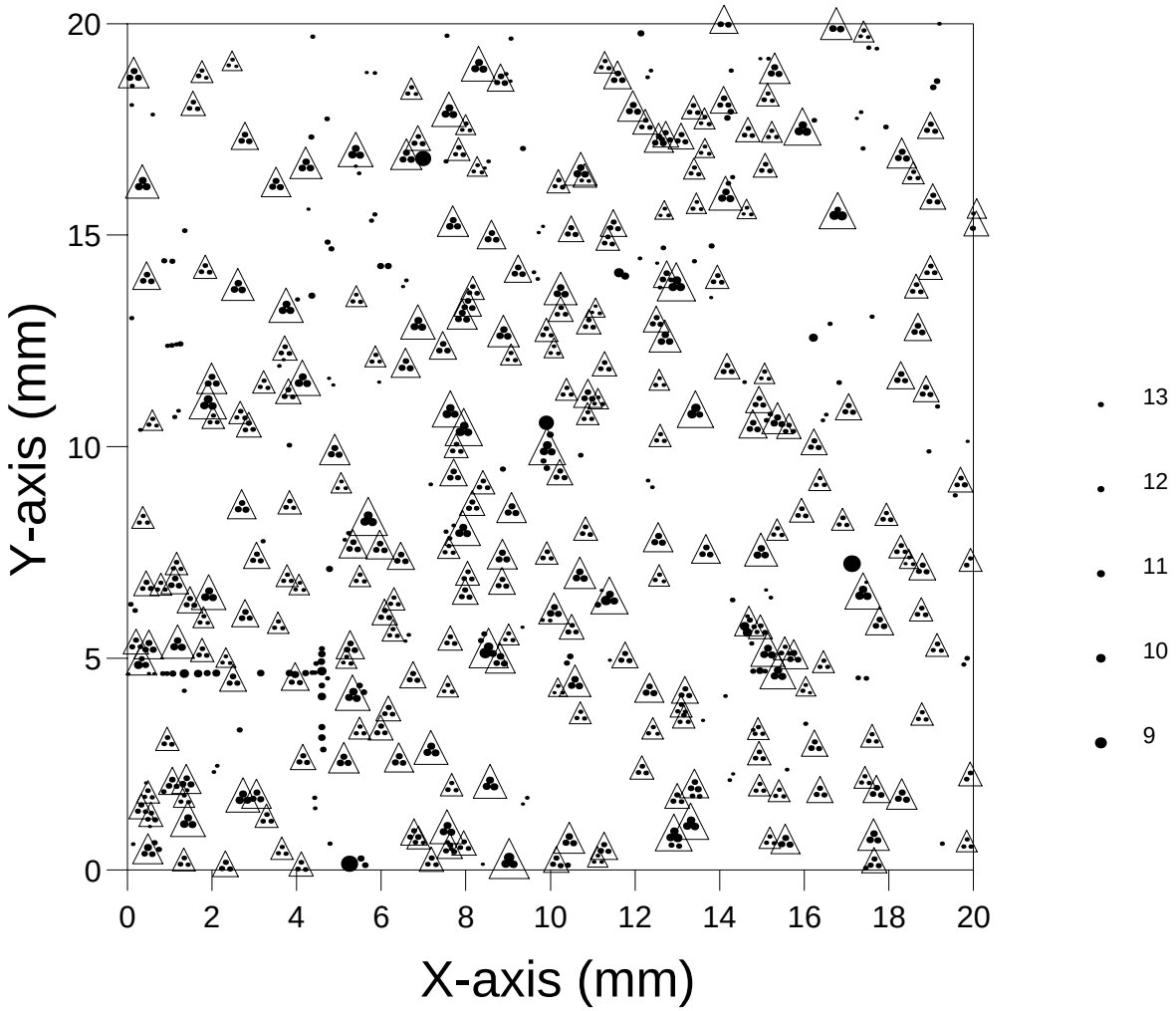

FIG. 1.—Catalog of the objects detected in a 20 by 20 cm area centered on NGC 6871 from a plate of Brussels Observatory, plotted with the B magnitudes derived from a calibration curve. The asterism provided by a triple exposure is used to identify stars and is defined by a triangle about 150 μm on a side. Optical double stars can be resolved when the angular separation is larger than $2''$–$3''$. Stellar flare candidates are identified when the flickering between the three stellar images of a candidate is larger than 0.4 mag. About 8% of the stars inventoried qualify for flare activity during the 20–30 minute exposure in one image.

3. KINEMATICAL CLASSIFICATION OF NEARBY DISK DWARFS

The comparison with modern digital sky surveys (Deutsch 1999) is made when using the Quick-V survey outputs provided by the GSC I (Lasker et al. 1990), and we compute an approximate color index $B-V$ and a proper-motion component that allow us to derive an approximate stellar surface temperature (by color index) and a stellar radius (by luminosity class derived from the reduced proper motion diagram). This classification is intended to provide a set of disk dwarfs in the greater solar neighborhood (Fresneau 1999, 154). A set of 2×10^5 stars (about 1 star out of 3) shows a significant total proper motion larger than $0''.02\ \mathrm{yr}^{-1}$ and is classified from the kinematics as a disk dwarf population.

The distribution of 16×10^3 stellar flare candidates (about 8% of the disk dwarf candidates) that have a significant magnitude scatter larger than 0.4 is presented as a function of $B-V$ in Figure 2 for the four test regions. We found that the plates with a 20 minute exposure appeared more sensitive to the flickering, especially for stars with $B-V \geq 1.2$, which is the domain of the nearby M dwarfs known for showing flares of large amplitude over some minutes in the B band. About 25 % of the stellar flare candidates in the four test regions include stars with $B-V \leq 0.4$, blueward of Parenago's discontinuity ($B-V = 0.61$), which suggests that we are dealing with relatively recently formed disk dwarfs. The large amplitude of the stellar flare candidates presently detected in the galactic anticenter direction in Gemini for stars with $B-V \leq 0.4$ (Fig. 2) is not investigated in the present study. We just want to point out that stars with $B-V \geq 1.0$ show about the same amplitude for the stellar flare candidates in all four test regions, suggesting that a selection based on photographic data, even rudimentary in the geometric and radiometric accuracies, appears sufficient to segregate stellar flare candidates of the same color (Bondar' 1995).

We know that the present kinematical classification cannot discriminate clearly between different types of eruptive variables that are intrinsically quite different over the range $0.0 \leq B-V \leq 1.2$. We wish to point out that the technique of analyzing the three exposures per photographic plate of a century-old survey can separate highly reddened variable stars and discover stellar flares just by the rapid (less than 20–30 minutes duration) flickering of light from these stars, as we conclude from the present analysis in four test regions.

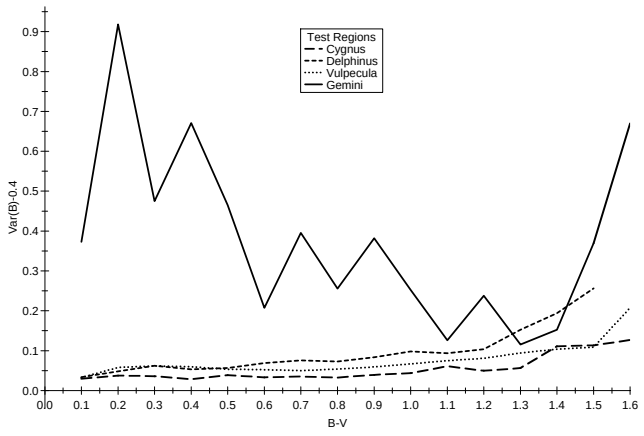

FIG. 2.—Stars with an excess of flickering in the B-magnitude scatter of 0.4 during the 20–30 minute exposure matched to the Quick-V survey plates used as second epoch. The mean value of the flickering excess to the 0.4 B-magnitude scatter for 16×10^3 stars with proper motion larger than $0''.02\ \mathrm{yr}^{-1}$ is plotted as function of the photographic color index $B-V$ in the four test regions. Stars redder than $B-V \sim 1.2$ appear in all four regions with a scatter in excess of 0.2 mag to the flickering of 0.4 mag. These stars qualify as nearby dMe candidates known for showing flare activity.

4. MASS ACCRETING PROCESS IN STELLAR FLARE CANDIDATES

Here we used the catalog of 5×10^5 stars detected by the fast measuring machines and identified by the triple exposures on the set of 130 astrographic plates. We matched the catalog with the Quick-V survey provided by GSC I for proper-motion and color index determination and we classified from the kinematics 2×10^5 stars as disk dwarfs. A significant magnitude variability larger than 0.4 is observed between the three exposures of 20–30 minutes of the astrographic plates for about 8% of the sample of suspected disk dwarfs. Our study is now restricted to this sample of 16×10^3 stars over the range $0.0 \leq B-V \leq 1.2$ with rudimentary observational photographic data interpreted within the framework of a kinematical classification that provides an absolute magnitude, a distance, a transverse velocity, and a general law for interstellar reddening (Fresneau & Monier 1999).

Since we know that flare stars are found in stellar aggregates (Aniol et al. 1990), our goal in the present study is to discriminate possible young pre–main-sequence (PMS) stars in the greater solar neighborhood that we may associate with nebulosities, even out of the regions of known stellar aggregates. Since we know that the flare stage can indicate stars in a post–T Tauri phase (Winterberg et al. 1995, 119), we can envision using the all-sky astrographic survey for star formation history analysis in the greater solar neighborhood. To study the effect of the interstellar medium (ISM) on the relative velocity of stars, we used the Lindblad diagram to estimate a variation of the angular momentum around the vertical axis of the galactic disk, since we know that the magnitude of the angular momentum is approximately conserved (see Figs. 3–5 in Binney & Tremaine 1987, 120).

The proper-motion components we derived in the present study are secular values since they are based on 100 year–old observations for the first epoch. They do not provide the instantaneous energy and angular momentum per unit mass, but they are sensitive to changes in these quantities (Odenkirchen & Brosche 1999). We want to correlate the variation of the angular momentum around the z-axis of the galactic disk with a possible mass loss or mass accretion due to the flaring activity that we observe on century-old plates. We know that a typical mass loss of $10^{-4}\ M_\odot\ \mathrm{yr}^{-1}$ can occur in FU Orionis–type stars dumping as much as $10^{-2}\ M_\odot$ onto the central star over 1 century (Kenyon, Hartmann, & Hewett 1988).

We know that a functional form is valid for the two integrals of motion, the binding energy, $E-U$ and the component of the angular momentum vector, L_z, that is parallel to the axis of symmetry of the Galaxy (Kalnajs 1976). Even if the two-integral model is inadequate for the Galaxy, we use the simple structure of an axisymmetric system since we are restricted to a close volume in which the angular momentum does not vary much along an orbit and

determines a unique relation between $E - U$ and L_z (Fresneau 1994). We will assume that the stellar flares associated with molecular cloud material show a kinematical signature in the Galactic potential variation due to the ISM. The scattering due to the ISM depopulates the orbits at the binding energy $E - U$ over a narrow range of L_z and moves the orbit to higher $E - U$ and smaller L_z, according to the relative rotation in the Galactic disk (Hori 1962). Since the changes in the quantities L_z and $E - U$ are related, we can look at the distribution of stars in $(L_z, E - U)$ space.

Figure 3 shows the Lindblad diagram for the stars in the Cygnus test region (*filled circles*) and in the Gemini test region (*open circles*), detected as disk dwarfs and showing a B-magnitude variability larger than 0.4 about a century ago. We plot along the x-axis the binding energy $E-U$, in units of 1000 (km s^{-1})^2, where E is the familiar kinetic energy $E = 1/2(u^2 + v^2 + w^2)$ where u, v, and w are the components of the velocity vector (Johnson & Soderblom 1987) derived from the proper-motion components and the kinematical distance, and U is the galactic potential (Carlberg & Innanen 1987), with a shape that can illustrate the same relationship as any other galactic potential.

We plot along the y-axis the square of the angular momentum, $L_z = (RV)^2$, in units of 100 (kpc km s^{-1})^2, where R is the cylindrical coordinate in the galactic plane and V the galactic velocity rotation at each stellar location. We assume, in view of the distribution between E and L_z, that L_z does not vary much along an orbit (Innanen & Papp 1977).

We observe on Figure 3 the locus of circular orbits that bounds the diagram along the isochrone galactic potential (Gerhard & Saha 1991) that links L_z and E, since an excess of disk dwarfs will follow such a trajectory in both regions. All stars plotted in Figure 3 have shown flares of short duration (less than 20 minutes) around a century ago. We cannot identify any particular type, since the character of the light curves cannot be ascertained. We derive the offset in the angular momentum from Figure 3 as the shift in the locus of circular orbits due to a possible binding energy offset, the result of a galactic potential variation in the closed volume under study. We assume that the galactic potential is not static over orbital timescales and that energy per unit mass and effective potential changes are due to environmental interactions.

For each star, we derive the offset $\mathscr{E}$ along the x-axis from the general trend between L_z and $E-U$ in each test region. We assume that $\mathscr{E}$ estimates the variation of the galactic potential due to the mass of the swept-up ISM. For each star that we classified as a disk dwarf, we derived a mass variation $\mathscr{M}$ from the two observations 100 years apart and from a mass-luminosity relation (Popper 1980). We speculate in the present analysis that ISM mass accreted by the star carries away the same specific angular momentum as that of the ISM it leaves, adding some amount of angular momentum to the stellar orbit in the equatorial galactic plane. We accommodate in the Lindblad diagram the presence of noncircular orbits as the result of this mass transfer phase.

To quantify this very crude recipe for selecting stellar flares associated with variation in mass transfer rate, we plot in Figure 4 the scatter of the binding energy offset $\mathscr{E}$ derived from the Lindblad diagram (in $10^6\ M_\odot$) as a function of the stellar mass variation $\mathscr{M}$ (in $10^{-2}\ M_\odot\ \mathrm{yr}^{-1}$) in the four test regions. The present statistical approach is designed only to study angular momentum loss and to identify the flares as a fraction of a star luminosity due to accretion or mass loss. The effect of angular momentum exchanges is assumed to result from the density gradient in the galactic potential due to small-scale ISM variations.

Since an accretion rate of $10^{-7}\ M_\odot\ \mathrm{yr}^{-1}$ can produce an accretion luminosity of 1 $L_\odot$ (Lynden-Bell & Pringle 1974), we would like to detect classical T Tauri star (cTTS) candidates. In the present study, we associate flares with variation in mass transfer rate in accretion disks. Only spectroscopic data will identify the components of the star and the steady state disk. The deductions are highly speculative but imply a possibility of detecting the signature of disks from a kinematical analysis of 100 year–old observations. We can estimate from Figure 4 the linear slope

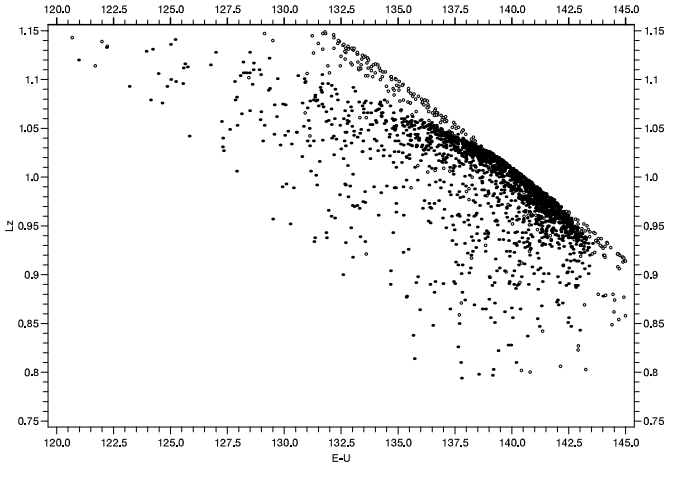

FIG. 3.—Lindblad diagram of stars with significant proper motion ($\geq 0\farcs02\ \mathrm{yr}^{-1}$) and with a detected flickering larger than 0.4 B magnitude in the Gemini (*open circles*) and in the Cygnus test regions (*filled circles*). The square of the angular momentum, L_z, in units of 100 (kpc km s^{-1})^2 is plotted on the y-axis, and the binding energy, $E-U$, in units of 1000 (km s^{-1})^2 is plotted on the x-axis. The shift along the x-axis from the curve of circular velocity is estimated as an offset in the disk potential U due to mass variation over the orbital timescales.

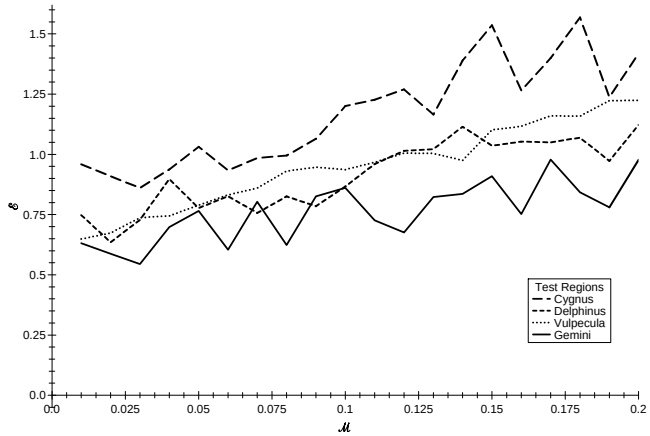

FIG. 4.—Autocorrelation between the potential offsets estimated from the Lindblad diagram plotted as a function of the separation in mass due to the observed flickering in B magnitude. The unit on the x-axis is $10^{-2}\ M_\odot\ \mathrm{yr}^{-1}$, and the unit on the y-axis is $10^6\ M_\odot$. We derive from the linear trend visible in the four regions $\dot{M} = \mathscr{M}/\mathscr{E} = 10^{-8}\ M_\odot\ \mathrm{yr}^{-1}$ to consider the mass variation between the two epochs of observations as a possible effect of mass transfer at a constant rate scaled to unit mass.

between the binding energy offset $\mathscr{E}$ (in $10^6\ M_\odot$) along the Y-axis and the stellar mass variation $\mathscr{M}$ (in $10^{-2}\ M_\odot\ \mathrm{yr}^{-1}$) along the X-axis, a mass accretion rate scaled to unit mass $\dot{M} = \mathscr{M}/\mathscr{E}$ of $10^{-8}\ M_\odot\ \mathrm{yr}^{-1}$, which is typical for classical T Tauri stars, with the assumption that the mass transfer rate is constant.

Since the stars under study are on the order of 1.5 $M_\odot$, we identify an approximate age for the stellar sample of 0.15 Gyr, with the assumption that the mass transfer rate of $10^{-8}\ M_\odot\ \mathrm{yr}^{-1}$ is constant. This lifetime ($\sim$1/2 galactic year) is typical of the young A–F stars in the solar neighborhood.

In this section, we explain mass loss by winds and mass transfer. We assume that the stars are interacting with a steady nonaxisymmetric potential disturbance rotating at the same angular rate, and we want to account for accretion as the source of luminosity activity in the flickering observed in the stars under study.

5. PHOTOELECTRIC U, B, AND V PHOTOMETRY OF PMS STELLAR CANDIDATES ALONG THE VULPECULA RIFT

As an example of the kinematical selection presented in the previous paragraphs, along with the sketch of a fully automated procedure using reduced proper motion diagrams and Lindblad diagrams dealing with the integrals of motions as natural coordinates, we show on Figure 5 the stellar mass variation, DM (in units of $10^{-2}\ M_\odot\ \mathrm{yr}^{-1}$), derived for a sample of 200 stars with significant flares versus the shift, DU_p (in units of $10^6\ M_\odot$), from the locus of circular orbits derived from the Lindblad diagram along the binding energy axis. These candidates are selected from a sample of 1000 targets according to their location within the interstellar dust that we identified with the Local spiral arm (Fresneau & Monier 1999). From Figure 5 we select the PMS candidates according to the two mass-loss rates scaled to unit mass (DM/DU_p): $2 \times 10^{-8}\ M_\odot\ \mathrm{yr}^{-1}$ for the stars along the eastern rim of the Vulpecula Rift (*filled circles*) and $5 \times 10^{-8}\ M_\odot\ \mathrm{yr}^{-1}$ for the stars along the western rim (*open circles*). We assume from Figure 5 that we identify two groups of stars according to the two different mass-loss rates that we would like to connect to the two rims of the Vupecula Rift associated with the Local spiral arm.

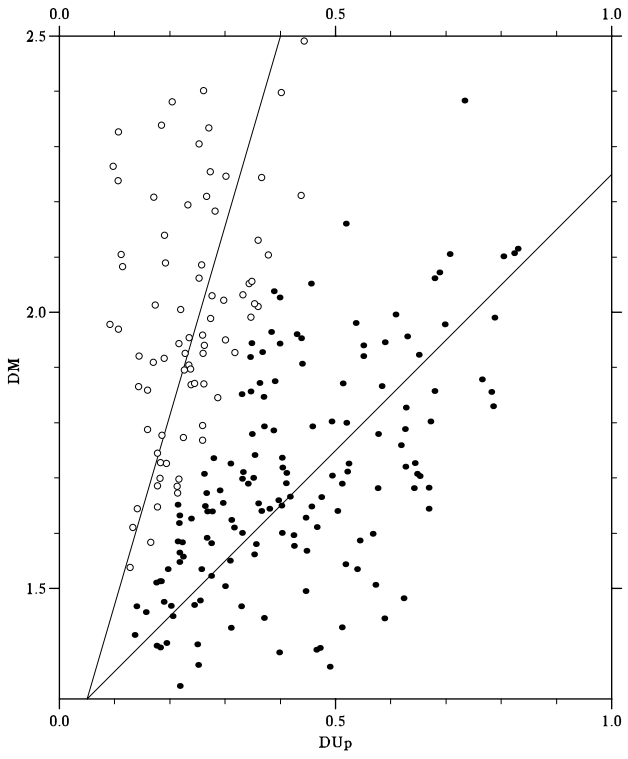

FIG. 5.—Selection of targets in the Vulpecula Rift according to two different accretion rates scaled to unit mass $\dot{M} = DU/DU_p = 2 \times 10^{-8}\ M_\odot\ \mathrm{yr}^{-1}$ for stars along the eastern rim (*filled circles*) and $5 \times 10^{-8}\ M_\odot\ \mathrm{yr}^{-1}$ for stars along the western rim (*open circles*) of the Vulpecula Rift. DM is the variation of mass, in units of $10^{-2}\ M_\odot\ \mathrm{yr}^{-1}$, detected from observations 100 years apart. DU_p, in units of $10^6\ M_\odot$, is the offset in the galactic potential estimated from a Lindblad diagram similar to the one of Fig. 3.

Photoelectric observations of the subset of 200 candidates were obtained at the 91 cm telescope of the Catania Astrophysical Observatory[4] (CAO). The photoelectric UBV photometry observations of the candidates were made in 1999 September and October by using the normal observational procedure relative to standard stars and applying the atmospheric extinction corrections in use at CAO. The standard stars were taken from the list of equatorial stars (Landolt 1983). Mean errors in photoelectric observations are in the 0.01–0.02 mag range.

We derived the absolute magnitude M_V by correcting the V photoelectric observed photometry from the absorption law of 1.5 mag kpc^{-1} with the distance derived from the kinematical analysis (Fresneau & Monier 1999). We applied the same corrections for distance and absorption to the UB photoelectric observations to get the dereddened intrinsic color indexes $(B-V)_0$ and $(U-B)_0$ for the sample of 200 stars. We applied a unique extinction law in the direction of the Vulpecula Rift and a unique absorption of 1.5 mag for the eastern and western rims of the rift.

In Figure 6 we plot the color-magnitude diagram, which shows a well-defined main sequence (Johnson & Morgan 1953) for stars along the two rims of the Vulpecula Rift and possible pre–main-sequence stars that are still on evolutionary tracks toward the main sequence. We suggest that stars along the western rim (*open circles*) are more evolved than stars along the eastern rim (*filled circles*), since most of the PMS stellar candidates out of the main sequence (about 10% of the entire set) belong to the eastern rim sample. We notice also that the turnoff point of the main sequence of the stars along the western rim is located at a brighter absolute magnitude, suggesting a sequential star formation between the eastern and western rims, since the Vulpecula Rift was identified with the Local spiral arm (Fresneau & Monier 1999).

We use this color-magnitude diagram to segregate evolved stellar candidates from possible PMS stars in estimating $D(B-V)$, the offset in $(B-V)_0$ of the stars from the main sequence (*solid line*) along the $(B-V)$ axis. We assume that if we correct the intrinsic color $(B-V)_0$ of a shift of $D(B-V)$, we need to correct the intrinsic $(U-B)_0$ of a shift of $0.72(U-B)_0$ along the $(U-B)$ axis, since we are dealing with an absorption law suitable for the entire region under study, the Vulpecula Rift.

When we plot on Figure 7 the $(U-B)_0$ versus $(B-V)_0$ for the two sets of stars segregated from Figure 6 and corrected

[4] See http://w3c.ct.astro.it/sln/index.html.

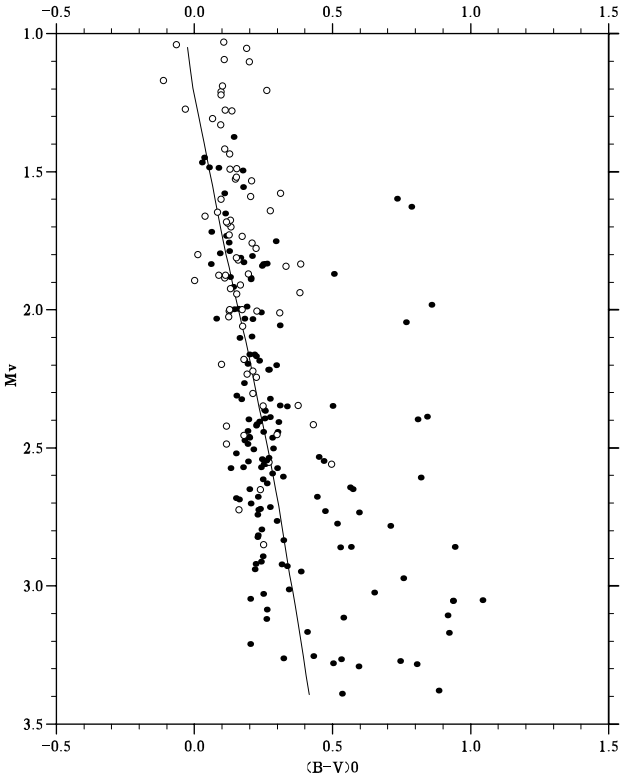

FIG. 6.—V and B photoelectric photometry dereddened in view of the kinematical distance derived from the reduced proper motion diagram, a total extinction in the Vulpecula Rift of 1.5 mag, and an extinction law of 1.5 mag kpc^{-1}, assumed to be similar along both rims. The stars along the eastern rim of the rift (*filled circles*) appear to be less evolved than the stars along the western rim (*open circles*) in view of the turnoff point along the main sequence. The shift in $(B-V)_0$ to the main sequence (*solid line*) is used to identify possible PMS star candidates. Most PMS candidates are located along the eastern rim, suggesting a sequential star formation.

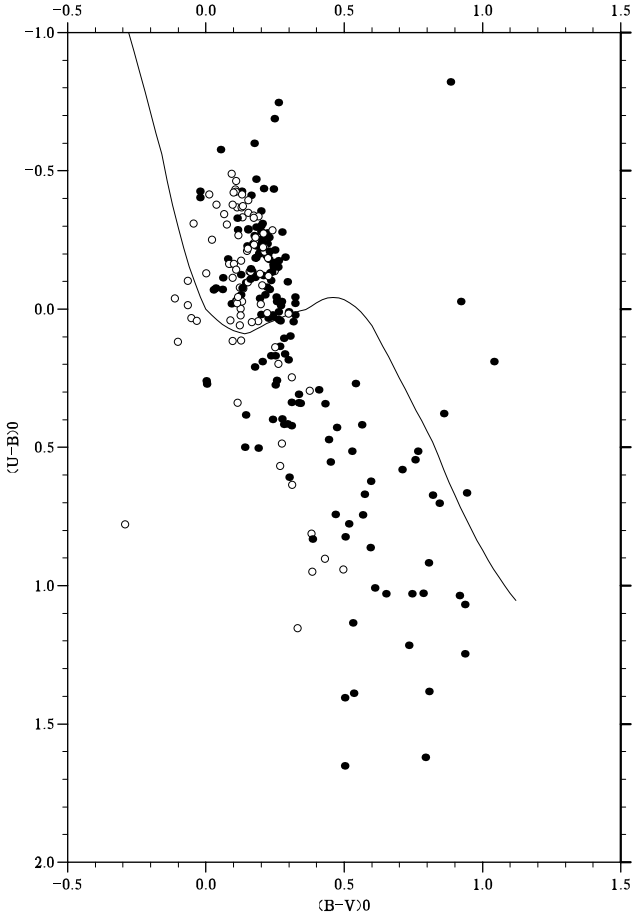

FIG. 7.— $(U-B)_0$ vs. $(B-V)_0$ diagram for the stars corrected from the shift in $D(B-V)_0$ derived from Fig. 6. The A–F disk dwarf candidates detected in Fig. 6 do not show the Balmer continuity that should be measured by the jump in $U-B$ of the main sequence (*solid line*). We presume that these stars are more luminous than normal stars. A shift in $(U-B)_0$ along the $(U-B)$-axis is derived and will be correlated with the shift in $(B-V)_0$ determined in Fig. 6.

from $D(B-V)$ and $D(U-B)$, we can observe that the Balmer discontinuity is not very well defined, suggesting that the A–F stars under study may well be hotter than the kinematical classification suggested. This could prove that their photospheric radiation fields tend to suppress the strong Balmer continuum, in particular for most of the stars located above and to the right of the main sequence (MS; *solid line*). Figure 7 is used to derive the appropriate offset $D(U-B)$ from the MS along the $(U-B)_0$ axis. At this point we have corrections $D(B-V)$ and $D(U-B)$ for the set of 200 stars that we would like to associate with some physical characteristics, since we deal with two groups of stars along two rims of the Vulpecula Rift, almost 100 pc apart (Fresneau & Monier 1999).

On Figure 8, we plot these corrections with the blackbody line, and we observe that most of the corrections $D(B-V)$ and $D(U-B)$ of the stellar candidates follow the blackbody line trend when another part of the corrections looks redder in the $(B-V)$ and bluer in the $(U-B)$, mostly for the eastern rim stars (*filled circles*). This effect suggests that we are dealing with two different mechanisms for stellar variability in these candidates and need further spectroscopic observations. Since we measure a color that turns bluer in $(U-B)$ when it turns redder in $(B-V)$ for about 10% of the 200 targets, we suggest that we can discriminate clearly between objects that are intrinsically quite different.

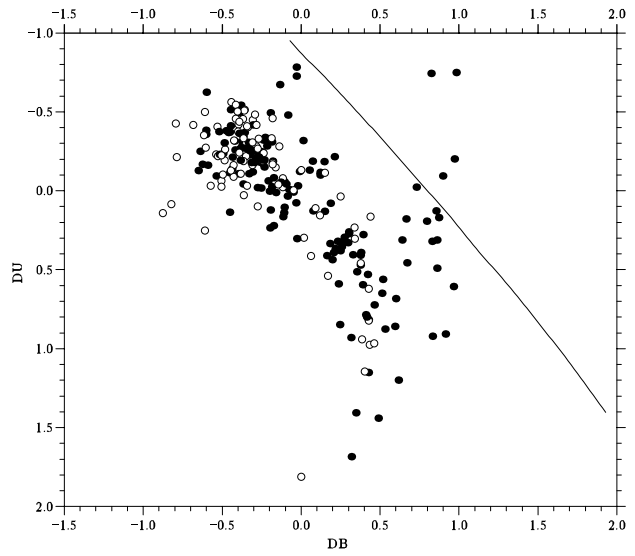

FIG. 8.—Shifts in $(B-V)_0$ measured on Fig. 6 along the $(B-V)$-axis, and in $(U-B)_0$ measured on Fig. 7 along the $(U-B)$-axis follow the general trend of the blackbody line (*solid line*). We notice that stars look redder in both color indexes, except for about 10% of the eastern rim stars (*filled circles*) that are redder in $(B-V)_0$ but bluer in $(U-B)_0$. We suggest two mechanisms for the signature of the flickering detected along the Vulpecula Rift.

A normal process for discriminating stellar flares is to consider that stars are redder when the circumstellar accretion disk is optically thin and bluer when the circumstellar accretion disk is optically thick.

The main point of the present section is the assumption that the kinematical classification provided by the reduced proper motion diagram and the Lindblad diagram applied to stellar flares detected in the solar neighborhood identifies two mechanisms in the physical process associated with these flares. Support to validate this very simple picture will need follow-up spectroscopic observations.

6. CONCLUSION

This paper makes use of a set of 130 photographic plates inherited from an all-sky survey that started in 1887 to provide star maps down to apparent magnitude 14.5. The technique of triple exposure designed for this photographic survey allows us to discriminate stars from plate defects and to detect stellar variability over the 20–30 minute exposure. Modern CCD observations could provide the very same information concerning the flickering of these stars, unless these targets are now in a quiescent phase. A great advantage of the 100 year–old observations is to provide first-epoch positions for deriving proper motion, thanks to modern-epoch surveys. A total proper-motion component of $0\farcs02\ \mathrm{yr}^{-1}$ is considered significant (Hoogerwerf & Blaauw 2000) and provides a way for analyzing a magnitude-limited sample (down to B magnitude 14.5 ± 1.5) to a distance-limited sample (up to about 250 pc).

We used fast measuring machines to produce a catalog of stellar images that we matched with modern surveys to select possible nearby A–F disk dwarfs from kinematic criteria. We restrict the sample of stars to those that show a magnitude variability larger than 0.4, which allows us to reject about 92% of the stars in the catalog and to start an observing program based on criteria that we would like to link to mass accretion of about $10^{-6}\ M_\odot$ over a century, typical for cTTS and Herbig Ae stars of about $1.5\ M_\odot$.

We used crude recipes for the many stages of selecting from the analysis of 100 year–old extensive photographic data the appropriate candidates in a possible mass transfer phase. The basic steps of our pragmatic approach can be fully automated to start a systematic search of old ($\sim 10^8$ yr) T Tauri stellar candidates near the zero-age main-sequence (ZAMS) (Feigelson 1996) or active coeval ZAMS stars, not necessarily PMS stars (Briceño et al. 1997), and to investigate some linear progression in sequential star formation over a large volume (Lépine & Duvert 1994). Our approach is different from the one that makes use of century-old observations to compute proper-motion components of known T Tauri stars still present in associations or to establish likely membership (Frink et al. 1997).

Photoelectric UBV photometry performed on 200 candidates of apparent magnitude 9–14 suggests that the success rate in detecting possible PMS stars is on the order of 10% with no clues to the nature of the candidates, but it indicates that accretion may be due to two different mechanisms, especially for stars located at the western and eastern rims of the Great Dark Rift in Vulpecula. We suspect that flares are prominent in the U band, but we lack sufficient observations to define any light curves of the objects under study or investigate whether a P Cygni profile in H_α is present in the majority of the PMS candidates.

We are grateful to R. Humphreys, M. Irwin, and J. Guibert for scanning 100 year–old astrographic plates with, respectively, the APS of Minnesota University in Minneapolis, the APM of the Institute of Astronomy in Cambridge (England), and the MAMA of Paris observatory. We thank S. Catalano for arranging the observing run at the 91 cm telescope of Catania Astrophysical Observatory and P. Kroll of Sonneberg Observatory for his useful comments as referee of this paper.

REFERENCES

Abad, C., & Vicente, V. 1999, A&AS, 136, 307
Aniol, R., Duerbeck, H. W., Seitter, W. C., & Tsvetkov, M. K. 1990, in IAU Symp. 137, Flare Stars in Star Clusters, Associations and the Solar Vicinity, ed. B. R. Pettersen, L. V. Mirzoyan, & M. K. Tsvetkov (Boston: Kluwer), 85
Bertin, E., & Arenouts, S. 1996, A&AS, 117, 393
Binney, J., & Tremaine, S. 1987, Galactic Dynamics (Princeton: Princeton Univ. Press)
Bondar', N. I. 1995, A&AS, 111, 259
Briceño, C., Hartmann, L. W., Stauffer, J. R., Gagné, M., Stern, R. A., & Caillault, J. P. 1997, AJ, 113, 740
Carlberg, R., G., & Innanen, K. A. 1987, AJ, 94, 666
Deutsch, E. W. 1999, AJ, 118, 1882
Feigelson, E. D. 1996, ApJ, 468, 306
Fresneau, A. 1990, AJ, 100, 1223
———. 1994, AJ, 108, 629
———. 1999, in Treasure Hunting in Astronomical Plate Archives, ed. P. Kroll, C. la Dous, & H. J. Bräuer (Frankfurt: Harri Deutsch)
Fresneau, A., & Monier, R. 1999, AJ, 118, 421
Frink, S., Röser, S., Neuhäuser, R., & Sterzik, M. F. 1997, A&A, 325, 613
Gerhard, O. E., & Saha, P. 1991, MNRAS, 251, 449
Hoogerwerf, R., & Blaauw, A. 2000, A&A, 360, 391
Hori, G. 1962, PASJ, 14, 353
Innanen, K. A., & Papp, K. A. 1977, AJ, 82, 322
Johnson, D. R. H., & Soderblom, D. R. 1987, AJ, 93, 864
Johnson, H. L., & Morgan, W. W. 1953, ApJ, 117, 313
Kalnajs, A. 1976, ApJ, 205, 751
Kenyon, S. J., Hartmann, L., & Hewett, R. 1988, ApJ, 325, 231
Landolt, A. U. 1983, AJ, 88, 853
Lasker, B., Sturch, C. R., McLean, B. J., Russell, J. L., Jenkner, H., & Shara, M. M. 1990, AJ, 99, 2019
Lépine, J. R. D., & Duvert, G. 1994, A&A, 286, 60
Luyten, W. J. 1949, ApJ, 109, 532
Lynden-Bell, D., & Pringle, J. E. 1974, MNRAS, 168, 603
Mouchez, E. 1887, Annuaire pour l'an 1887 par le Bureau des Longitudes (Paris: Gauthier-Villars)
Odenkirchen, M., & Brosche, P. 1999, Astron. Nachr., 320, 397
Ortiz-Gil, A., Hiesgen, M., & Brosche, P. 1998, A&AS, 128, 621
Popper, D. M. 1980, ARA&A, 18, 115
Turner, H. H. 1900, MNRAS Suppl., 60, 617
Urban, S. E., Corbin, T. E., Wycoff, G. L., Martin, J. C., Jackson, E. S., Zacharias, M. I., & Hall, D. M. 1998, AJ, 115, 1212
Winterberg, J., Nolte, M., Seitter, W. C., Duerbeck, H. W., Tsvetkov, M. K., & Tsvetkova, K. P. 1995, Lecture Notes in Physics, Vol. 454 (Berlin: Springer)